Tunable far-infrared laser spectroscopy of hydrogen bonds: The $K_a = 0(u) \rightarrow 1(g)$ rotation–tunneling spectrum of the HCl dimer

Geoffrey A. Blake[a)]
Division of Geological and Planetary Sciences, California Institute of Technology 170-25, Pasadena, California 91125

Kerry L. Busarow, R. C. Cohen, K. B. Laughlin, Y. T. Lee, and R. J. Saykally
Department of Chemistry and Materials and Chemical Sciences Division, University of California and Lawrence Berkeley Laboratories, Berkeley, California 94720

(Received 10 June 1988; accepted 16 August 1988)

The ground state $K_a = 0(u) \rightarrow 1(g)$ b-type subband of the rotation–tunneling spectrum of the symmetric ^{35}Cl–^{35}Cl, ^{37}Cl–^{37}Cl, and the mixed ^{35}Cl–^{37}Cl hydrogen chloride dimers have been recorded near 26.3 cm^{-1} with sub-Doppler resolution in a continuous two-dimensional supersonic jet with a tunable far-infrared laser spectrometer. Quadrupole hyperfine structure from the chlorine nuclei has been resolved. From the fitted rotational constants a $(H^{35}Cl)_2$ center-of-mass separation of 3.81 Å is derived for the $K_a = 1(g)$ levels, while the nuclear quadrupole coupling constants yield a vibrationally averaged angular structure for both tunneling states of approximately 20–25 deg for the hydrogen bonded proton and at least 70–75 deg for the external proton. This nearly orthogonal structure agrees well with that predicted by *ab initio* theoretical calculations, but the observed splittings and intensity alterations of the lines indicate that the chlorine nuclei are made equivalent by a large amplitude tunneling motion of the HCl monomers. A similar geared internal rotation tunneling motion has been found for the HF dimer, but here the effect is much greater. The ground state tunneling splittings are estimated to lie between 15–18 cm^{-1}, and the selection rules observed indicate that the *trans* tunneling path dominates the large amplitude motion, as expected, provided the dimer remains planar. From the observed hyperfine constants, we judge the dimer and its associated tunneling motion to be planar to within 10°.

INTRODUCTION

For over 70 years now the subject of van der Waals and hydrogen bonding has received a great deal of attention, with entire series of monographs being devoted to the subject.[1] The importance of these weak bonds emanates from their ubiquitous presence in condensed phases, especially in biological systems. Despite such enduring interest, a detailed understanding of intermolecular forces, in particular the nature of hydrogen bonding, has proved elusive. General advances in experimental chemical physics during the past decade have led to several new experimental techniques capable of addressing the study of intermolecular forces at a new level of detail. In this context, high resolution spectroscopy of small weakly bound clusters in the microwave and mid-infrared regions of the electromagnetic spectrum has been particularly significant. Experiments at these wavelengths probe the structure of a complex either via its rotational spectrum or the vibrational spectrum of one of the component monomers. The former method probes the very lowest region of the ground state potential energy surface, while the latter probes manifolds well above the dissociation energy of the adduct; neither is, in itself, a direct probe of the total ground state intermolecular potential, which is ultimately what is being sought in these experiments. Nevertheless, studies in the microwave region have been highly successful, resulting in the availability of structures for dozens of complexes.[2] Infrared spectroscopy, while less mature, is currently progressing rapidly.[3] The most direct route to the intermolecular potential requires analyses of the low frequency vibrations of the van der Waals and hydrogen bonds themselves, which occur in the far-infrared, a region which is only now becoming technologically accessible with the advent of sensitive, high resolution far-infrared laser spectrometers. The power of these new methods has been demonstrated in a recent series of experimental and theoretical papers on the far-infrared vibration–rotation spectra of the Ar–HCl system.[4–10]

A feature common to many spectra of weakly bound clusters at all wavelengths, provided sufficient resolution is employed, is tunneling splittings or perturbations induced by large amplitude zero-point motions of the monomers within the slowly varying intermolecular potential. When present they may be used to extract considerable dynamical information since substantial regions of the potential are explored. The first tunneling spectra to be recorded experimentally were those of the HF dimer in the pioneering molecular beam electric resonance (MBER) work of Dyke *et al.*[11] By examining the $J_{Ka} = 0_0 \rightarrow 1_0$ transitions of $(HF)_2$, $(DF)_2$, and HF–DF, Dyke *et al.* were able to demonstrate that the symmetric dimers undergo a large amplitude tunneling motion in which the free and hydrogen bonded protons or deuterons are exchanged. Since this early experiment, numerous papers have appeared on the HF dimer including extensions of the microwave measurements,[12–14] study of the infrared spectra of the free and hydrogen bonded HF stretches,[15] FTIR spectroscopy of the fundamental intermolecular tor-

[a)] Berkeley Miller Postdoctoral Fellow.

 0021-9606/88/236577-11$02.10 © 1988 American Institute of Physics

Downloaded 08 Mar 2006 to 131.215.225.174. Redistribution subject to AIP license or copyright, see http://jcp.aip.org/jcp/copyright.jsp

sional vibration near 400 cm^{-1},[16] papers describing the group theoretical interpretation of the observed spectra and their relation to the symmetries of the potential energy surface,[17,18] analyses of the Born–Oppenheimer breakdown of the monomer/adduct motions,[19] and *ab initio* calculations on the structure and energetics of the dimer.[20–25] Of the theoretical investigations of the HF dimer, the significant effort by Dykstra and Truhlar[25] to fit a global intermolecular potential is especially noteworthy. Such intense interest in this species exists because it is easily studied both experimentally and theoretically and because it serves as a useful prototype for models of hydrogen bonding.

Ab initio and empirical theoretical studies of the hydrogen halide dimers all predict an asymmetric, planar, nearly orthogonal *equilibrium* structure with a slightly nonlinear hydrogen bond and an external proton bond angle between 60°–90°.[20–24] The equilibrium angle of the hydrogen bond is near 5°–10° for all dimers, including mixed forms such as HF–HCl, but the external angle is found to vary dramatically with different monomers. For example, the external bond angle in the HF dimer is predicted to be 62°, in good agreement with experiment, but the same angle in the HCl dimer is predicted to be nearly 87°. Large amplitude zero-point motions in these complexes distort the experimentally determined, and vibrationally averaged, structures significantly from their equilibrium configurations. For example, in most of the hydrogen halide dimers the predicted potential energy surfaces have steep angular wells in the planar coordinates, resulting in nonequivalent halogen and hydrogen nuclei in the equilibrium geometry. Tunneling of the light hydrogen nuceli in the HF dimer, and by inference in other symmetrical weakly bound complexes as well, averages the asymmetric environments of the free and hydrogen bonded monomers to produce apparently equivalent hyperfine splittings and line intensities in the rotation and vibration–rotation spectra of the adduct.

Studies of the spectra of other hydrogen halide dimers would clearly provide an interesting series of test cases for examining the variation of hydrogen bond properties with electronegativity, electronic structure, mass, etc. The heavier HCl and HBr dimers also have the advantage of at least two naturally abundant isotopes of the halide nuclei possessing easily resolvable nuclear hyperfine structure, which provide useful structural and dynamical constraints. While Janda *et al.*[26] have described MBER work on the mixed HF–HCl dimer and Bumgarner and Kukolich[27] have reported a microwave FTS study of the HI–HF complex, surprisingly, only one paper on the high resolution spectrum of the isolated HCl dimer exists, an analysis of the infrared HCl stretching vibrations by Ohashi and Pine.[28] Since this work was carried out in static low temperature cells with substantial pressure and Doppler broadening, no resolution of the hyperfine structure was possible, but it illustrates why, in fact, no microwave spectra have been reported. Whereas the tunneling splitting in (HF_2) is on the order of 20 GHz, the analogous splitting in the HCl dimer is estimated to be at least several wave numbers.[28] As we shall describe later, both rotational and vibrational transitions must sample states *across* the tunneling splitting for most of the likely tunneling paths; that is, no pure rotational spectrum exists. Indeed, if the tunneling splitting is large enough no microwave transitions will be present even for dimers with small rotational constants. Another general feature of hydrogen bonded dimers is the large value of their A rotational constant–usually on the order of a few to several tens of wave numbers–which means that b-type transitions always occur well into the far-infrared, even in the absence of tunneling. It is precisely these b-type bands which allow the determination of the A rotational constants, and it is for such reasons that complete experimental structures do not exist for even the simplest species.

Thus, for hydrogen bonded dimers both the vibration–rotation spectra and the rotation–tunneling spectra will often occur predominantly in the far-infrared. As mentioned above, few high resolution spectrometers are capable of working in this region. We have previously reported the construction of a tunable far-infrared laser spectrometer/two-dimensional free jet van der Waals cluster source and its initial application to the Σ bending vibration–rotation spectrum of Ar–HCl near 23.6 cm^{-1}.[9,10] We describe here the detection and analysis of another type of far-infrared mode in hydrogen bonded complexes, in this case the b-type $K_a = 0(u) \rightarrow 1(g)$ subband of the rotation–tunneling spectrum of the HCl dimer. The rotational and hyperfine constants derived from the analysis of such bands yield important constraints on the structure of weakly bound complexes and the nature of hydrogen exchange tunneling dynamics. For example, although low frequency observations of the water dimer have produced crude estimates of the tunneling–rotation interactions in this complex,[29] the direct measurement of the variation of such effects with quantum state is possible only in the far-infrared.[30]

EXPERIMENTAL

The data presented in this paper were taken with the Berkeley tunable far-infrared/two-dimensional supersonic expansion spectrometer, which is described in detail in previous papers.[9,10] Figure 1 presents a schematic diagram of the system. In brief, the source consists of a 1.5 in. $\times$ 0.001 in. two-dimensional stainless steel slit housed in a large vacuum chamber. The supersonic flow is maintained by a 2850 cfm roots blower (Edwards EH4200) backed by two 175 cfm mechanical pumps (Edwards E2M275). The total pumping speed is throttled to approximately 1600 cfm at chamber pressures in the several hundred mTorr range by the 40 ft $\times$ 8 in. PVC pipe which connects the vacuum chamber to the roots blower. Typical operating conditions were 500–600 Torr behind the nozzle with a background pressure in the chamber of approximately 100–130 mTorr. The same mix used in the Ar–HCl experiments (1%–3% HCl in Ar) produced very intense signals from the HCl dimer as well. We estimate roughly 0.1%–1% of the available HCl is in the form of dimers. As noted in our previous papers, two-dimensional nozzles have the distinct advantage over pinhole expansions of greatly increasing the sensitivity of direct absorption spectroscopy by increasing the (pathlength) $\times$ (density) product tremendously while si-

Downloaded 08 Mar 2006 to 131.215.225.174. Redistribution subject to AIP license or copyright, see http://jcp.aip.org/jcp/copyright.jsp

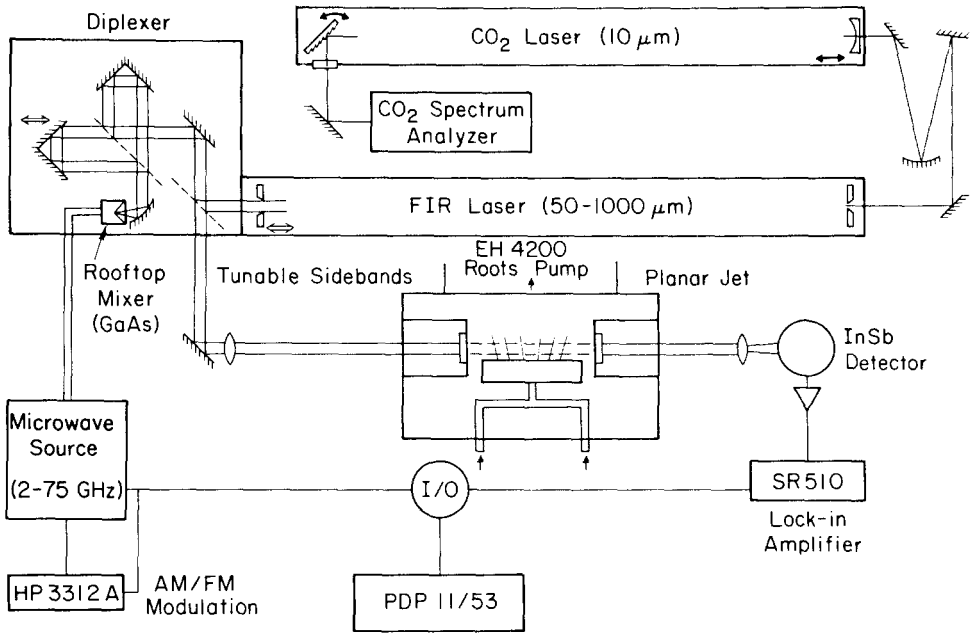

FIG. 1. Schematic diagram of the UCB tunable far-infrared/two-dimensional free jet spectrometer.

multaneously reducing the Doppler linewidths by about one order of magnitude. The overall increase in sensitivity relative to one-dimensional expansions with the same nozzle cross section is at least a factor of 100, and the sub-Doppler linewidths enable many fine structure or hyperfine splittings to be resolved even at far-infrared wavelengths. Linewidths in this study ranged from 300 to 400 kHz, with about 75 kHz of this broadening from time-of-flight effects and most of the remainder from residual Doppler motions and the modulation scheme used to record the spectra, or from pressure broadening in the jet core. Definitive assignments of the importance of each of these effects to the total linewidths observed await further detailed studies at shorter wavelengths. In similar experiments on the vibration–rotation–tunneling spectrum of Ar–H_2O near 21 and 25 cm^{-1} the measured intensity of the $H_2{}^{18}O$ $1_{01} \rightarrow 1_{10}$ transition at 547.676 GHz gives total densities of $\sim 10^{15}$ cm^{-3} in the probed region of the jet.[31] At these densities pressure broadening will contribute less than 100 kHz to the overall linewidth.

The highly monochromatic FIR radiation required for these experiments was produced by mixing the output from a longitudinally pumped FIR molecular laser with that from a commercial YIG-tuned microwave oscillator (HP 8673B). A commercial 150 W line tunable CO_2 laser (Apollo model 150) provides the IR pump radiation which drives a 2.3 m shop-built FIR laser. The 394 μm formic acid line (rest frequency = 761.6083 GHz[32]) was used to record the HCl dimer spectra. Instantaneous bandwidths of optically pumped FIR lasers are estimated to be only a few hundred Hertz for lasing molecules which are asymmetric tops, and the short term stability is known to be better than 50 kHz.[33] By incorporating commercial doublers into the microwave design (Spacek Ka2X, Honeywell V2200N), which are followed or driven by a Hughes 8001H12 traveling wave tube amplifier, the 2–26 GHz range of the HP8673B is extended to 75 GHz. This allows a 150 GHz region to be covered with a single laser setting if both first order sidebands are used. Strong absorbers in the jet have been observed on up to the seventh microwave sideband harmonic, and for such transitions the scanning range of the spectrometer is nearly 10 cm^{-1}. Spectra are recorded by frequency modulation of the microwave source with synchronous second harmonic detection. Because the lines are so narrow, very small FM deviations may be used, resulting in source amplitude fluctuations well below the detector noise of the spectrometer. On the strongest FIR laser lines approximately 100–200 μW of tunable radiation is produced in the 30 cm^{-1} region which passes directly through the free jet expansion before detection with a liquid helium cooled InSb hot electron bolometer (Cochise Instruments). For typical detector sensitivities of $10^{-(12-13)}$ $W/Hz^{1/2}$ this implies a power/noise ratio exceeding 10^5 for an integration time of 1 s. In dimers such as Ar–HCl, HCl–HCl, or Ar–H_2O where the transition moments are ~ 1 D, the stronger transitions absorb at least 0.1% of the sideband power, and the resulting signal to noise ratios are quite large (> 1000). A demonstration of the the sensitivity and resolution of the spectrometer/free jet source is presented in Fig. 2, a recording of the $R[0(u) \rightarrow 1(g)]$ transition of $(H^{35}Cl)_2$. The total scan width is 30 MHz and the peak fractional absorbance is near 10^{-3}, with a lock-in time constant of 300 ms.

Laser carrier radiation is separated from the tunable sidebands using a polarizing Michelson interferometer, but otherwise no extra filtering is employed. Both sidebands therefore pass through the jet, and when features are recorded there is always an ambiguity about which sideband is responsible for the absorption. By "pulling" the FIR laser frequency slightly to the red or to the blue through an adjustment of the laser cavity the sidebands may be easily separated as they move in opposite directions. For example, if the cavity length is increased the laser frequency decreases, and to synthesize the same *absolute* laser sideband frequencies requires a corresponding decrease or increase of the microwave setting on the lower and upper sidebands, respectively.

Downloaded 08 Mar 2006 to 131.215.225.174. Redistribution subject to AIP license or copyright, see http://jcp.aip.org/jcp/copyright.jsp

Because the laser frequency is not locked, however, great care must be exercised when retuning the laser to the peak of its gain curve. For the present measurements it is this resetting of the laser which dominates the uncertainties in the absolute measurements of the line positions. We estimate this uncertainty to be about 0.5–1.0 MHz. Certain HCl dimer transitions lie close to accurately calibrated lines of Ar–HCl,[10] and we have used these lines as secondary calibration standards. Since not all lines are calibrated, the overall rms deviation in the fit lies between the best that can be achieved (~ 50 kHz) and the laser pulling uncertainty noted above. Nuclear quadrupole hyperfine structure is recorded on a single pass, and is not affected by the laser pulling tests. Uncertainties in the quadrupole constants are determined primarily by the linewidths of the observed transitions, which are substantially sub-Doppler, and by short term drifts of the FIR laser caused by thermal effects and feedback between the two laser cavities. The fitted uncertainties in these constants are near 50–100 kHz (1σ).

ROTATIONAL ASSIGNMENTS AND SPECTRAL CONSTANTS

Several scans taken of the Ar–HCl Σ bending transitions taken under conditions described by Busarow *et al.*[9,10] also contained intense, unidentified features with considerable internal structure. The narrow linewidths of these features indicated that they arose within the free jet source, and the complicated splittings were suggestive of a molecule containing at least two chlorine nuclei. A complete survey of the region around the 394 μm formic acid line revealed the upper laser sideband spectrum shown in Fig. 2 along with a more detailed presentation of the $R(0)$ transition. The region between 740 and 760 GHz on the lower laser sideband, not plotted in Fig. 2, is blocked by atmospheric water vapor in the unpurged optical path. What remains is an orderly spectrum with clearly defined P, Q, and R branches of a nearly symmetric, prolate top. The splittings between the line clumps and the relative intensities of the lines within the clumps were both suggestive of a complex containing only two chlorine nuclei. With equivalent nuclei, the expected intensity ratio is roughly 10:6:1 in the 35/35, 35/37, and 37/37 forms, neglecting nuclear spin weights, for a natural ^{35}Cl/^{37}Cl ratio of 3:1.

By far the most convincing information regarding the identity of the unknown lines were their complicated hyperfine splittings. In several cases progressions could be followed over several J values even before absolute rotational assignments were made. Lower J lines tend to have the most complicated patterns while high J lines collapse to symmetrical triplet patterns, indicating that the coefficients leading the hyperfine energy level expressions differ in the upper and lower state. Figure 3 shows a series of hyperfine patterns for the H^{35}Cl dimer Q branch; similar spectra are observed for the other isotopic dimers. The high J hyperfine patterns are remarkably similar to those of methylene dichloride,[34] and since HCl is the only source of chlorine in the jet, $(HCl)_2$ is the most obvious prolate top. Initial rotational assignments confirmed this assumption based on ground state constants

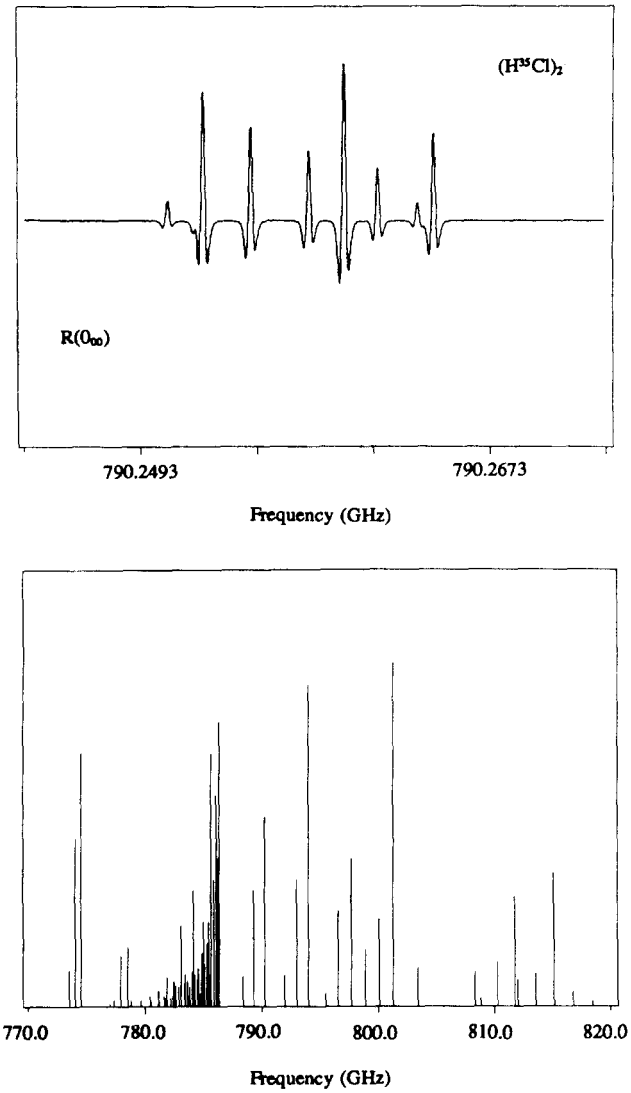

FIG. 2. Tracing of the $(H^{35}Cl)_2$ $R(0)$ transition, and a stick diagram of the lines observed from all three dimer isotopic combinations on the upper laser sideband.

extracted from the work of Ohashi and Pine.[28] Further support for the assignment of the bands to $(HCl)_2$ arises from the observed intensity alterations of the lines from the isotopically symmetric species. The spin 3/2 of the chlorine nuclei combined with the spin 1/2 of the hydrogen nuclei generate expected intensity alterations of 36:28 in the absence of resolved hyperfine structure, close to that detected.

Upon closer inspection of Fig. 2 it is apparent that, despite adequate experimental sensitivity, the $P(1)$ transitions are not observed while those of $R(0)$ are. Thus, the observed band has a perpendicular character, that is $\Delta K_a = 1$. Further, since $R(0)$ is present it must be a $K_a = 0 \rightarrow 1$ band, which would be allowed by either a b- or c-type dipole moment. To fit the observed transitions the standard rotational Hamiltonian for a nearly prolate asymmetric top must be supplemented with nuclear quadrupole and tunneling terms, and constants must be allowed to differ for the upper and lower state. For the HCl dimer the total Hamiltonian takes the form

Downloaded 08 Mar 2006 to 131.215.225.174. Redistribution subject to AIP license or copyright, see http://jcp.aip.org/jcp/copyright.jsp

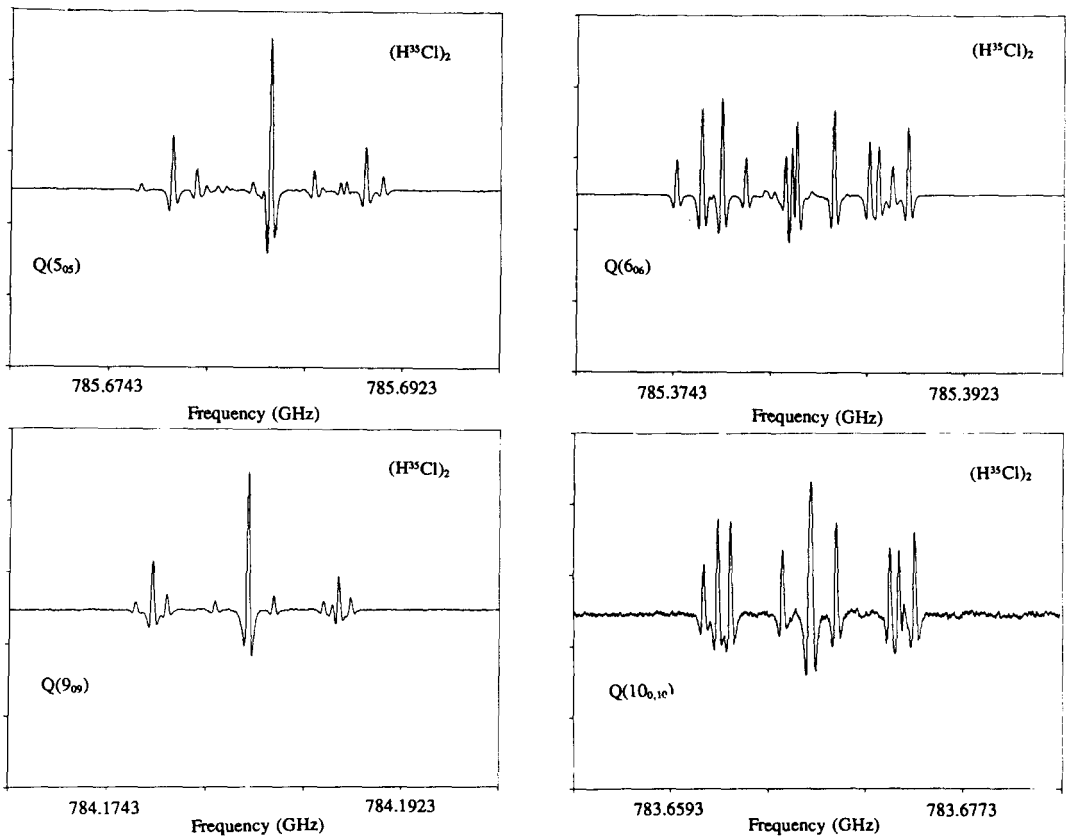

FIG. 3. Tracings of several Q-branch transitions of $(H^{35}Cl)_2$ illustrating the collapse of the hyperfine structure into symmetrical triplets, and the intensity alteration of even and odd J transitions.

$$H = H_R + H_Q + H_T, \tag{1}$$

where H_R and H_Q are the usual rotational and hyperfine terms, and H_T accounts for any tunneling perturbations. Quadrupole structure in the HCl dimer is complicated by the presence of two nuclei with $I = 3/2$ which, *a priori*, need not be equivalent. We have employed the $|I_1 J F_1 I_2 F M_F\rangle$ coupling scheme where the rotational quantum number J couples with one of the nuclear spins I_1 to create an intermediate F_1 quantum number, which then couples with the second nuclear spin I_2 (much smaller hyperfine structure resulting from the spin–rotation interactions of the hydrogen spins are unimportant at our current resolution) to produce the final quantum number F.

As noted in the Introduction, the HCl dimer undergoes a large amplitude hydrogen exchange tunneling motion similar to that observed in $(HF)_2$, which splits every rotational level into symmetric and antisymmetric tunneling states. The symmetry labeling of the individual tunneling–rotation eigenstates is best understood using the molecular symmetry groups.[35] As discussed by Dyke *et al.*[11] for the HF dimer, in this case the group contains the identity operator E, the only *feasible* permutation P_{12} which interchanges the hydrogen and chlorine nuclei simultaneously, the space-fixed inversion operator E^*, and the permutation–inversion operator $P_{12}^* = E^* P_{12}$. We follow the notation of Howard, Dyke, and Klemperer[12] and use the superscripts $+$ and $-$ to denote the state symmetry under E^* and the labels g or u to identify the symmetry under P_{12}. Values of the limiting prolate asymmetric top quantum numbers K_a are also listed as subscripts.

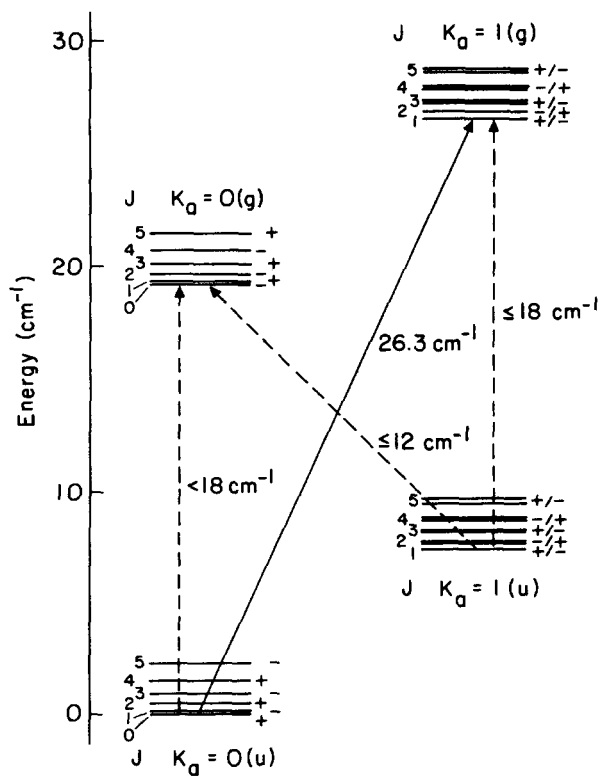

FIG. 4. Energy level diagram of the lowest rotation–tunneling levels of the HCl dimer, along with the observed band (solid line) and other allowed transitions (dotted lines).

Downloaded 08 Mar 2006 to 131.215.225.174. Redistribution subject to AIP license or copyright, see http://jcp.aip.org/jcp/copyright.jsp

For electric dipole transitions the selection rules are $+ \Leftrightarrow -$ and $g \Leftrightarrow u$. It is the $g \Leftrightarrow u$ selection rule that prohibits the observation of a pure rotational spectrum. Figure 4 presents an energy level diagram of the $K_a = 0,1$ states of the HCl dimer, outlining the symmetry properties of the rotation–tunneling states, the transitions allowed (dashed lines), and the states observed (solid lines) in this work.

Rough values for the rotational constants were obtained by fitting the average centers of the hyperfine multiplets, while initial values of the hyperfine constants were derived from the $R(0)$ line and several high-J Q-branch transitions. The $R(0)$ line is particularly useful as it involves hyperfine constants from only the upper state. These rough constants were used as input into Pickett's general vibration–rotation program capable of fitting spectra of asymmetric tops in up to nine vibrational states with four spins of arbitrary degeneracy.[36] In the current version of the program, it is not possible to enforce, *a priori*, strict equivalence of the hyperfine parameters for different nuclei. The individual coupling constants of each nucleus must be fit separately, and the degree of equivalence is determined entirely by the quality of the data. Initial predictions of the program were used to assign the complicated hyperfine patterns of the low-J transitions. A complete listing of only the hyperfine corrected transition frequencies and their assignments is presented in Table I, as a presentation of all the observed hyperfine components would require unreasonable space. The assignment of the observed transitions to a b-type, rather than a c-type, band is based on a comparison of the Q-branch spacings. For a b-type subband the $Q(J) - Q(J-1)$ spacing is given by $2J[\Delta_{10}(B+C)/2 + (B-C)/4]$, while in a c-type subband the same spacing is given by $2J[\Delta_{10}(B+C)/2 - (B-C)/4]$ [$\Delta_{10}(B+C)/2$ is the difference between the rotational constants in the upper and lower states].

Since we observe only a single b-type subband, a rigorous separation of the tunneling frequency and the A rotational constants for the upper and lower state is not possible. A rough separation of the two constants is provided by the quadrupole coupling constants of the chlorine nuclei if one assumes the total field gradient is unchanged from that in free HCl. For now, we have modeled the HCl dimer in an analogous fashion employed in analyses of spectra from ammonia and the hydronium ion: we assume a single tunneling frequency for all K_a states exists and fit separate rotational constants for the upper and lower state. It is quite likely, however, that the tunneling frequency depends strongly on the value of K_a,[12,13] and this approach will have to be generalized as further bands are analyzed. Indeed, from the estimated rotational constants and *ab initio* estimates of the binding energy we find that while the upper tunneling state energy is small with respect to the potential well, it may be a substantial fraction of the tunneling barrier–which implies that large changes in the tunneling splittings might well occur for different K_a levels. Our current best estimate of the positioning of the various rotation–tunneling states for $K_a = 0,1$ is depicted in Fig. 4.

In the ground state only the average rotational constant $\overline{B}_{0,u} = (B_{0,u} + C_{0,u})/2$ and the a-axis projection of the hyperfine constants $eqQ_{aa,u}$ may be determined, but in the upper state both the sum and difference of the A, B, and C rotational constants along with the a, b, and c axis projections of the quadrupole constants are involved. Only the $eqQ_{aa,g}$ projection and the difference between the bb and cc components of eqQ may be formally determined for $K_a = 1$, with the Laplace equation ($eqQ_{aa} + eqQ_{bb} + eqQ_{cc} = 0$) required to separate the individual projections. Distortion constants up to sixth order were required, in addition to the larger rotational and quadrupole constants, to fit the lines to within the estimated observational error. The rms residuals for the three isotopic species lie between 150 and 450 kHz, limited mainly by uncertainties in the unlocked laser frequency. Both Watson A- and S-reduced Hamiltonians were employed to fit the data in order to test correlation effects among the various parameters, and both models worked equally well. We find the hyperfine constants for the two chlorine nuclei are equivalent within experimental error in the symmetric dimers, and furthermore, no interactions involving the hydrogen spins were required. Table II presents a listing of the S-reduced constants for the various isotopic combinations. Although a rigorous structure cannot be derived for the dimer at this stage, the rotational and hyperfine constants determined are consistent with the known properties of the HCl monomers and a reasonalbe vibrationally averaged structure for the dimer, which we discuss next.

STRUCTURE OF THE DIMERS

The coordinate system used for our discussion of the structure of the HCl dimer is indicated in Fig. 5, along with estimates for the vibrationally averaged center of mass separation and hydrogen bonded and free HCl angles. The axis drawn in Fig. 5 connects the monomer centers of mass and is therefore not isotope invariant. However, the angular deviation of this axis from both the true a-inertial axis and the axis through the two chlorine nuclei is less than 0.5°. Corrections to the effective constants and bond angles are therefore quite small, and are well below other sources of error. As Howard, Dyke, and Klemperer[12] note, the derivation of a true equilibrium structure from the experimentally determined, vibrationally averaged rotational constants is not possible due to the effect of large amplitude motions in the complex. For all hydrogen halide dimers the four intermolecular degrees of freedom involve the planar orientation angles θ_1 and θ_2, the dihedral angle ϕ, and the center of mass separation R. Significant anharmonic terms exist along each coordinate, and it is also likely that strong angular/radial coupling occurs. Because the chlorine nuclei lie virtually on the a-axis, the average values of the various coordinates do not change markedly with Cl isotopic substitution, hence isotope effects can be used to place constraints on the equilibrium structure of the dimers.

For example, if the dimer is assumed to have a planar structure, the center of mass separation between the two HCl subunits may be derived from the equation (which is independent of the monomer orientations)

$$\mu r_0^2 = (h/8\pi^2 c)[C^{-1} - B_1(\mathrm{HCl})^{-1} - B_2(\mathrm{HCl})^{-1}], \quad (2)$$

where $\mu = M_1(\mathrm{HCl})M_2(\mathrm{HCl})/[M_1(\mathrm{HCl}) + M_2(\mathrm{HCl})]$ is

Downloaded 08 Mar 2006 to 131.215.225.174. Redistribution subject to AIP license or copyright, see http://jcp.aip.org/jcp/copyright.jsp

TABLE I. Hyperfine corrected HCl dimer transition frequencies (MHz).

J'	Ka_1	Kc'	v_1	J''	Ka''	Kc''	v''	Expt. freq.	Calc. freq.	Diff.
$(H^{35}Cl)_2$										
13	1	13	1	14	0	14	0	726 181.511	726 181.463	0.048
12	1	12	1	13	0	13	0	730 889.746	730 889.897	−0.151
10	1	10	1	11	0	11	0	740 125.329	740 125.325	0.004
9	1	9	1	10	0	10	0	744 651.178	744 651.181	−0.003
1	1	1	1	2	0	2	0	778 591.636	778 592.096	−0.460
17	1	16	1	17	0	17	0	778 839.185	778 839.212	−0.027
16	1	15	1	16	0	16	0	779 673.818	779 673.879	−0.061
13	1	12	1	13	0	13	0	781 894.523	781 894.441	0.082
12	1	11	1	12	0	12	0	782 538.901	782 538.961	−0.060
11	1	10	1	11	0	11	0	783 135.023	783 135.107	−0.084
10	1	9	1	10	0	10	0	783 682.659	783 682.594	0.065
9	1	8	1	9	0	9	0	784 181.176	784 181.156	0.020
7	1	6	1	7	0	7	0	785 030.957	785 030.565	0.392
6	1	5	1	6	0	6	0	785 381.123	785 381.001	0.122
3	1	2	1	3	0	3	0	786 133.288	786 133.272	0.016
1	1	0	1	1	0	1	0	786 384.453	786 384.434	0.019
1	1	1	1	0	0	0	0	790 258.089	790 258.094	−0.005
2	1	2	1	1	0	1	0	794 016.230	794 015.975	0.255
3	1	3	1	2	0	2	0	797 707.811	797 708.170	−0.359
4	1	4	1	3	0	3	0	801 334.405	801 334.536	−0.131
6	1	6	1	5	0	5	0	808 389.081	808 389.317	−0.236
7	1	7	1	6	0	6	0	811 817.354	811 817.547	−0.193
8	1	8	1	7	0	7	0	815 179.934	815 179.576	0.358
9	1	9	1	8	0	8	0	818 475.355	818 475.354	0.001
$(H^{35}Cl$–$H^{37}Cl)$										
10	1	10	1	11	0	11	0	740 563.459	740 563.242	0.217
9	1	9	1	10	0	10	0	744 963.462	744 963.751	−0.289
1	1	1	1	2	0	2	0	777 983.373	777 983.458	−0.085
11	1	10	1	11	0	11	0	782 418.342	782 418.299	0.043
9	1	8	1	9	0	9	0	783 432.383	783 432.966	−0.583
6	1	5	1	6	0	6	0	784 597.322	784 596.458	0.864
1	1	0	1	1	0	1	0	785 569.675	785 568.977	0.698
1	1	1	1	0	0	0	0	789 340.209	789 340.383	−0.174
2	1	2	1	1	0	1	0	793 000.023	792 999.978	0.045
3	1	3	1	2	0	2	0	796 596.163	796 596.328	−0.165
4	1	4	1	3	0	3	0	800 129.155	800 129.318	−0.163
7	1	7	1	6	0	6	0	810 346.726	810 346.948	−0.222
8	1	8	1	7	0	7	0	813 625.252	813 625.291	−0.039
9	1	9	1	8	0	8	0	816 839.944	816 839.626	0.318
$(H^{37}Cl)_2$										
1	1	1	1	2	0	2	0	777 368.096	777 368.588	−0.492
13	1	12	1	13	0	13	0	780 530.490	780 530.446	0.044
12	1	11	1	12	0	12	0	781 136.167	781 136.293	−0.126
11	1	10	1	11	0	11	0	781 696.724	781 696.480	0.244
10	1	9	1	10	0	10	0	782 210.699	782 210.839	−0.140
9	1	8	1	9	0	9	0	782 679.485	782 679.190	0.295
8	1	7	1	8	0	8	0	783 101.283	783 101.349	−0.066
7	1	6	1	7	0	7	0	783 476.617	783 477.136	−0.519
6	1	5	1	6	0	6	0	783 806.491	783 806.379	0.112
5	1	4	1	5	0	5	0	784 088.692	784 088.916	−0.224
4	1	3	1	4	0	4	0	784 324.904	784 324.601	0.303
3	1	2	1	3	0	3	0	784 514.026	784 513.308	0.718
2	1	1	1	2	0	2	0	784 655.753	784 654.933	0.820
1	1	0	1	1	0	1	0	784 750.039	784 749.395	0.644
1	1	1	1	0	0	0	0	788 419.947	788 419.070	0.877
2	1	2	1	1	0	1	0	791 980.216	791 980.397	−0.181
3	1	3	1	2	0	2	0	795 480.203	795 480.613	−0.410
4	1	4	1	3	0	3	0	798 919.597	798 919.716	−0.119
7	1	7	1	6	0	6	0	808 870.936	808 870.115	0.821
8	1	8	1	7	0	7	0	812 064.276	812 064.370	−0.094
9	1	9	1	8	0	8	0	815 196.857	815 197.102	−0.245

the dimer reduced mass as determined by the total masses of the individual HCl monomers, r_0 is the zero-point center of mass separation of the dimer, C is the rotational constant about the axis normal to the plane of the dimer, and B_1(HCl) and B_2(HCl) are the monomer rotational constants. Note that this equation may not be used for the $K_a = 0$ state since the B and C constants are not separately determinable. However, from the observed similarity of the

Downloaded 08 Mar 2006 to 131.215.225.174. Redistribution subject to AIP license or copyright, see http://jcp.aip.org/jcp/copyright.jsp

TABLE II. *S*-reduced HCl dimer constants (MHz).

Parameter	$K_a = 0(u)(2\sigma)$	$K_a = 1(g)(2\sigma)$
$(H^{35}Cl)_2$		
$(B + C)/2$	1 944.386 0(520)	1 915.496 0(550)
$(B - C)/4$	...	3.769 31(58)
D_J	0.008 82(45)	0.007 80(47)
H_J	− 0.156(130)E − 05	− 0.154(130)E − 05
$eqQ_{aa}(Cl_1)$	− 11.519(131)	− 13.624(179)
$eqQ_{aa}(Cl_2)$	− 11.529(131)	− 13.609(179)
$(eqQ_{bb} - eqQ_{cc})(Cl_1)$	...	− 49.436(640)
$(eqQ_{bb} - eqQ_{cc})(Cl_2)$	...	− 49.456(635)
$d(eqQ_{bb} - eqQ_{cc})(Cl_1)$	...	0.640(413)E − 02
$d(eqQ_{bb} - eqQ_{cc})(Cl_2)$	...	0.632(413)E − 02
$A_{eff} + \Delta_{tun}$	788 350.186(250)	...
$(H^{35}Cl\text{–}H^{37}Cl)$		
$(B + C)/2$	1 892.859 9(350)	1 864.939 9(360)
$(B - C)/4$	...	3.572 03(216)
D_J	0.006 45(53)	0.005 67(55)
H_J	− 0.853(265)E − 05	− 0.807(267)E − 05
$eqQ_{aa}(Cl_1)$	− 11.244(441)	− 13.232(582)
$eqQ_{aa}(Cl_2)$	− 8.658(445)	− 10.042(601)
$(eqQ_{bb} - eqQ_{cc})(Cl_1)$	...	− 48.476(647)
$(eqQ_{bb} - eqQ_{cc})(Cl_2)$	...	− 38.364(713)
$A_{eff} + \Delta_{tun}$	787 482.610(505)	...
$(H^{37}Cl)_2$		
$(B + C)/2$	1 841.759 5(516)	1 814.675 8(559)
$(B - C)/4$	...	3.458 98(179)
D_J	0.001 98(127)	0.000 82(130)
H_J	− 0.151(50)E − 04	− 0.159(55)E − 04
$eqQ_{aa}(Cl_1)$	− 9.055(112)	− 10.820(107)
$eqQ_{aa}(Cl_2)$	− 9.055(112)	− 10.820(107)
$(eqQ_{bb} - eqQ_{cc})(Cl_1)$	...	− 38.696(431)
$(eqQ_{bb} - eqQ_{cc})(Cl_2)$	...	− 38.696(438)
$A_{eff} + \Delta_{tun}$	786 611.316(550)	...

chlorine nuclear quadrupole hyperfine constants (see below), it is likely that the structure of the dimer is quite similar in the lower and upper tunneling state. From the fitted constants we find a nearly constant separation of 3.8139, 3.8145, and 3.8148 Å for the ^{35}Cl, mixed, and ^{37}Cl dimers in the $K_a = 1(g)$ state. Ohashi and Pine[28] find a slightly smaller separation of 3.797(1) Å for the $K_a = 1(u)$ lower tunneling state. Extrapolating the separation to infinite mass gives equilibrium separations between 3.75 and 3.79 Å, noticeably larger than the HF dimer separation of 2.72 Å.[12] Applications of the above equation to H/D isomers in $(HF)_2$ give a much larger scatter in the estimated separation, indicative of the marked radial/angular coupling noted previously and the strong effects of zero-point vibrational averaging on the experimentally derived structures. Because the chlorine nuclei lie so much closer to the center of mass these effects are much reduced in $(HCl)_2$, and consequently it is not possible to say much about the nature of such coupling with the present data set.

A better measure of the angular structure of the dimer, and some measure of the stretch/bend coupling in $(HCl)_2$, is provided by the quadrupole coupling constants of the chlorine nuclei, which are well determined by the present data set. The first point to note is that in the unmixed dimers the two nuclei are equivalent, which implies either the dimer has a single symmetric structure, or that if an asymmetric equilibrium structure exists, it is averaged to a symmetrical one by tunneling on a time scale of the rotation period. In the $K_a = 0$ stack only the a-axis projection of the quadrupole constant contributes to the hyperfine energies, but in the $K_a = 1$ upper tunneling state all three projections may be measured. If complex formation does not affect the field gradients at the chlorine nuclei then the expression

$$eqQ_{aa} + eqQ_{bb} - eqQ_{cc} = eqQ_{HCl} \tag{3}$$

would hold for each nucleus (the Laplace equation is always satisfied). We find, in fact, that the components in the dimer only add up to approximately 92% of the uncomplexed HCl quadrupole moment. A similar, but slightly larger, change is noticed in the deuterium substituted HF dimers, which have approximately twice the binding energy of the HCl dimer. Thus, most of the reduction in the effective dimer quadrupole moments are probably caused by vibrational averaging, and not by actual changes in the field gradient induced by hydrogen bond formation. We can correct for such effects quite accurately using the standard equation

$$[eqQ_{xx}]_{dimer} = [eqQ]_{monomer}\langle(3\cos^2\theta_{av,xx} - 1)/2\rangle \tag{4}$$

Downloaded 08 Mar 2006 to 131.215.225.174. Redistribution subject to AIP license or copyright, see http://jcp.aip.org/jcp/copyright.jsp

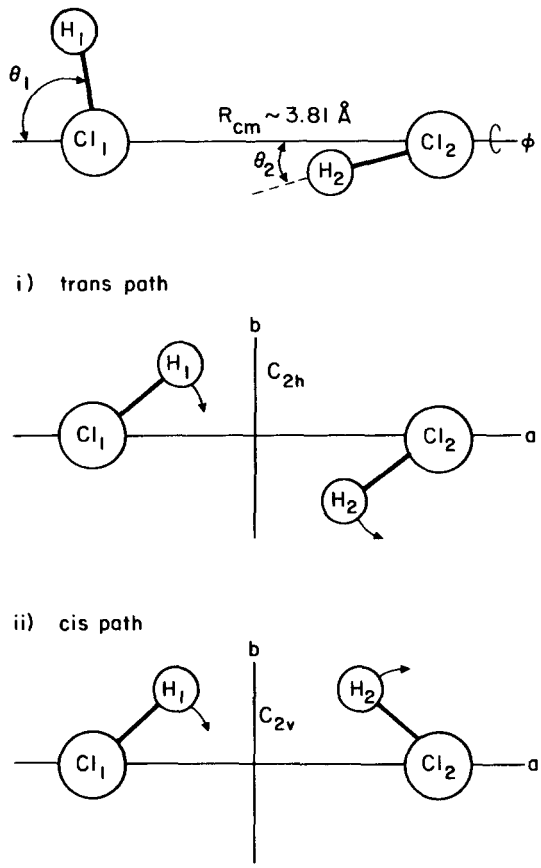

FIG. 5. Illustration of the coordinate system used to describe $(HCl)_2$ and its associated tunneling motion. Transition states for the planar *trans* and *cis* paths are also shown.

to account for the vibrational averaging and to derive *averaged* values for the in-plane angular coordinates.

Because of the tunneling motion, the observed quadrupole constants average over both the free and hydrogen bonded environments, that is

$$\langle(3\cos^2\theta_{\rm av} - 1)/2\rangle = 1/2[\langle(3\cos^2\theta_1 - 1)/2\rangle + \langle(3\cos^2\theta_2 - 1)/2\rangle]. \quad (5)$$

As Fig. 5 indicates, we use θ_1 for the free HCl angle and θ_2 for the hydrogen bonded HCl angle. Application of Eq. (4) yields averaged values near $\theta_{\rm av} = 47°$ for both K_a stacks and for all isotopes. The corresponding angle in the HF dimer is closer to 40°. The observed increase in the a-axis projection of the chlorine quadrupole constant in the upper tunneling state translates into only a 1.5° decrease in the average in-plane angle $\theta_{\rm av}$. Such a large value of the average angle demands that the vibrational zero-point hydrogen bond angle be at least 15° (for which the acute external HCl angle is 90°). Even for hydrogen bonded angles as large as 35°, the external proton angle is approximately 60°. Thus, the HCl dimer is considerably more orthogonal than $(HF)_2$, as predicted by several theoretical calculations. "Rotational saturation," in which the free monomer bond angle swings out towards an orthogonal position as the rotational energy increases, and which is observed to be quite significant in the HF dimer, should not be especially severe in this case, since the free HCl monomer is already nearly orthogonal to the a axis in the ground state. Outward rotation of the complexed HCl monomer is also possible, but should occur much more slowly because of the greater restoring force of the hydrogen bond. To gain any further insight into the vibrationally averaged structure in the HCl dimer it will be necessary to study the deuterated forms in the hope that, as in the HF dimer, the large amplitude tunneling motion can be restricted and coupling constants for the individual nuclear sites obtained.

The magnitude and sign of the c-axis projection of the chlorine nuclear quadrupole constant calculated from the Laplace equation yields an expectation value of the dihedral angle of $\langle\phi\rangle = 15°$. Vibrational averaging of the second Legendre coefficient of the hyperfine expressions produces observed angles which may differ substantially from their true equilibrium values. For angles near $\pi/2$, $\cos\theta$ is nearly a linear function of θ and the vibrationally averaged constant closely approximates the equilibrium value. Near $\theta = 0$, however, the averaged and equilibrium angles are better related by the expression

$$\theta_{\rm obs} = (\theta_e^2 + \Delta\theta^2)^{1/2}, \quad (6)$$

where θ_e is the equilibrium value and $\Delta\theta$ is the rms amplitude. For both $(HF)_2$ and HF–HCl $\Delta\theta$ is close to 20°.[13,26] With similar amplitudes for the HCl dimer, the likely equilibrium values for the hydrogen bonded proton lie between 0° and 15°, with external angles between 70° and 85°. Similarly, for rms amplitudes between 10° and 20° in the out-of-plane coordinate ϕ, the deviation of the dimer from planarity is less than 5°. Both electrostatic and simple HOMO–LUMO arguments lead to such orthogonal structures for the HCl dimer due to the large electric quadrupole interactions involved, and can explain in a qualitative way the observed structural trends in the hydrogen halide dimers.[21,22] Table III lists the vibrationally averaged and estimated equilibrium angles for the three observed isotopic forms of the HCl dimer and the estimated equilibrium structure of the HF and HF–HCl dimers.

TUNNELING MECHANISMS AND THE INTERMOLECULAR POTENTIAL

From the observed nuclear quadrupole constants and the inferred structure for the dimers we estimate a value near 7.5 cm^{-1} for the A rotational constant of the HCl dimer in both the upper and lower tunneling states, assuming a rigid

TABLE III. Structural constants for HCl–HCl, HF–HCl, and HF–HF.

Parameter	HCl–HCl $K = 0$	HCl–HCl $K = 1$	HF–HCl (Ref. 26)	HF–HF (Refs. 11 and 12)
R_{cm}		3.81	3.40	2.79
$\theta_{\rm av}$	48.0° ± 2°	46.8° ± 2°		40° ± 1°
θ_1(vib)	~70°–80°	~70°–80°	50° ± 5°	61° ± 5°
θ_2(vib)	⩾15°	⩾15°	21° ± 5°	23° ± 5°
ϕ(vib)		10° ± 2°		
θ_1(eq)	70°–80°	70°–80°	49° ± 2°	60° ± 2°
θ_1(eq)	0°–10°	0°–10°	6.5° ± 2.5°	7° ± 3°
ϕ(eq)		⩽10°		

Downloaded 08 Mar 2006 to 131.215.225.174. Redistribution subject to AIP license or copyright, see http://jcp.aip.org/jcp/copyright.jsp

structure. The inversion motion is likely to increase the value of A, and we use the above as a lower limit. Increases to values as high as 8–11 cm^{-1} are possible. Since the observed band origin is the sum of the tunneling splitting for $K_a = 1$ and the A rotational constant of the lower tunneling state, this gives a tunneling splitting of 15–18 cm^{-1} in the $K_a = 1$ stack. Similar, but slightly smaller, values are expected for $K_a = 0$. Thus, except for radio frequency transitions within a hyperfine multiplet all rotation–tunneling transitions will lie well above the microwave frequency range unless accidental degeneracies occur between opposing tunneling states, or unless the complex is nonplanar. Hougen and Ohashi[37] have presented detailed arguments concerning the probable selection rules for various *planar* tunneling paths of the HF dimer. The two extreme paths considered are a *trans* path leading to a C_{2h} transition configuration and a *cis* path which produces a C_{2v} transition state (see Fig. 5). The *trans* path should possess a much lower tunneling barrier and is therefore the most intuitively appealing mechanism. Basically, Hougen and Ohashi find that for $\Delta K_a = 0$ (a-type) bands both tunneling paths produce selection rules which require transitions across the tunneling splitting. For $\Delta K_a = \pm 1$ (b-type or c-type) bands, however, the *trans* model also imposes transitions *across* the tunneling splittings, while the *cis* path allows pure rotational transitions. To assign our observed b-type band to a pure rotational $K_a = 0 \rightarrow 1$ band or to the $K_a = 0(g) \rightarrow 1(u)$ band (whose band origin lies at $|A_{\text{eff}} - \nu_{\text{tun}}|$) would require an A rotational constant of at least 26 cm^{-1}, which is totally incompatible with the observed hyperfine constants. In addition, the out of plane modes are predicted to have c-type symmetry while stretching vibrations will have a-type symmetry, leaving only the in plane rotation–tunneling modes. While we cannot rule out either the *cis* model or nonplanar tunneling mechanisms completely, we feel the observed selection rules and rotation–tunneling constants strongly support the *trans* model of Hougen and Ohashi[37] constructed for the HF dimer.

With this interpretation of the data, we predict that the a-type bands for the $K_a = 0$, 1 stacks should lie between 15 and 18 cm^{-1} and the $K_a = 1(u) \rightarrow 0(g)$ band should lie near 8–12 cm^{-1}. Positions of some of the other vibration–rotation and rotation–tunneling bands may be crudely estimated from the observed distortion constants. For example, the quartic constant D_J is simply one-half the change in $(B + C)/2$ upon end over end rotational motion. Some of this constant arises from bend/radial coupling, but most of it arises from stretching of the hydrogen bond. The Kratzer relation ($\omega^2 = 4B^3/D_J$) may be used to determine the harmonic stretching frequency ω and the stretching force constant k_S. The three isotopic combinations give a hydrogen bond stretching frequency between 60 and 65 cm^{-1} and a stretching force constant ranging from 0.0395 to 0.050 mdyn/Å. For Ar–HCl the same quantities are 32.4 cm^{-1} and 0.0117 mdyn/Å. If one assumes a Lennard-Jones potential for the "radial" coordinate a dissociation energy (D_e) of approximately 500 cm^{-1} is derived. From a series of well calibrated pressure dependent absorption measurements Pine and Howard derive a hydrogren bond (D_0) energy of 431 ± 22 cm^{-1}.[38] Large amplitude tunneling effects render such crude, but simple, analyses of the bending coordinates inappropriate. Analysis of deuterated forms of the HCl dimer may provide a better handle on the in-plane bending forces through the large expected changes in the tunneling splittings. Out-of-plane modes of the HCl monomers would lie near the uncomplexed HCl $J = 0 \rightarrow 1$ transition at 21 cm^{-1} for low barrier heights, but will move to shorter wavelengths as the barriers are increased. McKellar and coworkers[39] have detected several bands near 160 cm^{-1} using Fourier transform spectroscopy on a low temperature static hydrogen chloride gas cell, and have assigned these bands to the out of plane motion of the HCl dimer and to higher K components of the rotation-tunneling spectrum. The analysis of this mode will give useful information about the dihedral coordinate ϕ. We note for now that the large value of its band origin is consistent with steep angular wells in the ϕ coordinate and with the planar structure inferred from the chlorine eqQ_{cc} nuclear quadrupole constants. The FTS A constant of 10.96 cm^{-1} shows the expected tunneling–rotation modifications of the average dimer structure derived from the hyperfine constants discussed above.

To summarize, sub-Doppler rotation–tunneling spectra of the HCl dimer have been recorded with a tunable far-infrared laser/continuous two-dimensional free jet spectrometer. Three overlapping rotation/tunneling bands near 26 cm^{-1} have been observed and assigned to the $K_a = 0(u) \rightarrow 1(g)$ states of the $^{35/37}Cl$ pure and mixed isotopic forms. Resolution of the chlorine quadrupole patterns yields estimates of the structure and tunneling systematics of the dimers. A center of mass separation near 3.81 Å is found with an estimated equilibrium structure of about 0°–15° for the hydrogen bonded proton and a nearly orthogonal position of at least 70°–80° for the external proton. The observed position, selection rules, and hyperfine constants of the bands strongly favor an in-plane *trans* tunneling path with tunneling splittings near 15–18 cm^{-1}. Observations of other rotation–tunneling bands and rotation–vibration transitions of the HCl dimer and similar bands of deuterated forms such as HCl–DCl and $(DCl)_2$ will be required to unambiguously determine the equilibrium structure and the associated intermolecular potential. The deduced rotational and distortion constants should be most useful in constructing quantitative semiempirical models of the intermolecular potential energy surface like those that have proved quite successful for simpler systems such as Ar–HCl, and for comparing with results from *ab initio* calculations of the structure and bonding in hydrogen halide dimers.

ACKNOWLEDGMENTS

This work was supported by the Director, Office of Energy Research, Office of Basic Energy Sciences, Chemical Sciences Division of the U. S. Department of Energy under Contract No. DE-AC03-76SF00098. The FIR laser system was funded by the National Science Foundation (Grant CHE-8612296) and by the Army Research Office–University Research Instrumentation Program (Grant DAAL03-86-G-0184). The authors thank H. M. Pickett for useful discussions and for providing the multispin Hamiltonian

Downloaded 08 Mar 2006 to 131.215.225.174. Redistribution subject to AIP license or copyright, see http://jcp.aip.org/jcp/copyright.jsp

program. G. A. B. gratefully acknowledges financial support from the Berkeley Miller Basic Research Institute.

[1] *The Hydrogen Bond*, edited by P. Schuster, G. Zundel, and G. Zandorfy (North-Holland, Amsterdam, 1976).
[2] T. R. Dyke, Topics Current Chem. **120**, 85 (1984).
[3] R. E. Miller, J. Phys. Chem. **90**, 3301 (1986); C. M. Lovejoy and D. J. Nesbitt, Rev. Sci. Instrum. **58**, 807 (1987).
[4] D. Ray, R. L. Robinson, D. H. Gwo, and R. J. Saykally, J. Chem. Phys. **84**, 1171 (1986).
[5] R. L. Robinson, D. Ray, D. H. Gwo, and R. J. Saykally, J. Chem. Phys. **87**, 5149 (1987).
[6] R. L. Robinson, D. H. Gwo, D. Ray, and R. J. Saykally, J. Chem. Phys. **86**, 5211 (1987).
[7] R. L. Robinson, D. H. Gwo, and R. J. Saykally, J. Chem. Phys. **87**, 5156 (1987); Mol. Phys. **63**, 1021 (1988).
[8] J. M. Hutson, J. Chem. Phys. **89**, 4550 (1988).
[9] K. L. Busarow, G. A. Blake, K. B. Laughlin, R. C. Cohen, Y. T. Lee, and R. J. Saykally, Chem. Phys. Lett. **141**, 289 (1987).
[10] K. L. Busarow, G. A. Blake, K. B. Laughlin, R. C. Cohen, Y. T. Lee, and R. J. Saykally, J. Chem. Phys. **89**, 1268 (1988).
[11] T. R. Dyke, B. J. Howard, and W. Klemperer, J. Chem. Phys. **56**, 2442 (1972).
[12] B. J. Howard, T. R. Dyke, and W. Klemperer, J. Chem. Phys. **81**, 5417 (1984).
[13] H. S. Gutowsky, C. Chuang, J. D. Keen, T. D. Klots, and T. Emilsson, J. Chem. Phys. **83**, 2070 (1985).
[14] W. J. Lafferty, R. D. Suenram, and F. J. Lovas, J. Mol. Spectrosc. **123**, 434 (1987).
[15] A. S. Pine and W. J. Lafferty, J. Chem. Phys. **78**, 2154 (1983).
[16] K. von Puttkamer and M. Quack, Mol. Phys. **62**, 1047 (1987).
[17] A. S. Pine, W. J. Lafferty, and B. J. Howard, J. Chem. Phys. **81**, 2939 (1984).
[18] A. E. Barton and B. J. Howard, Faraday Discuss. Chem. Soc. **73**, 45 (1982).
[19] I. M. Mills, J. Phys. Chem. **88**, 532 (1984).
[20] D. R. Yarkony, S. V. O'Neil, H. F. Schaefer III, C. P. Baskin, and C. F. Bender, J. Chem. Phys. **60**, 855 (1974).
[21] C. Girardet, A. Schriver, and D. Maillard, Mol. Phys. **41**, 779 (1980).
[22] M. Allavena, B. Silvi, and J. Cipriani, J. Chem. Phys. **76**, 4573 (1982).
[23] J. F. Gaw, Y. Yamaguchi, M. A. Vincent, and H. F. Schaefer III, J. Am. Chem. Soc. **106**, 3133 (1984).
[24] D. W. Michael, C. E. Dykstra, and J. M. Lisy, J. Chem. Phys. **81**, 5998 (1984).
[25] C. E. Dykstra and D. G. Truhlar, J. Chem. Phys. **88**, 1786 (1988).
[26] K. C. Janda, J. M. Steed, S. E. Novick, and W. Klemperer, J. Chem. Phys. **67**, 5162 (1977).
[27] R. E. Bumgarner and S. G. Kukolich, J. Chem. Phys. **86**, 1083 (1987).
[28] N. Ohashi and A. S. Pine, J. Chem. Phys. **81**, 73 (1984).
[29] L. H. Coudert, F. J. Lovas, R. D. Suenram, and J. T. Hougen, J. Chem. Phys. **87**, 6290 (1987).
[30] K. L. Busarow, R. C. Cohen, G. A. Blake, K. B. Laughlin, Y. T. Lee, and R. J. Saykally (in preparation).
[31] R. C. Cohen, K. L. Busarow, K. B. Laughlin, G. A. Blake, M. Havenith, Y. T. Lee, and R. J. Saykally, J. Chem. Phys. **89**, 4494 (1988).
[32] M. Inguscio, G. Moruzzi, K. M. Evenson, and D. A. Jennings, J. Appl. Phys. **60**, R161 (1986).
[33] J. Farhoomand and H. M. Pickett, Int. J. Infrared. Millimeter Waves **8**, 441 (1987).
[34] R. J. Myers and W. D. Gwinn, J. Chem. Phys. **20**, 1420 (1952).
[35] H. C. Longuet-Higgins, Mol. Phys. **6**, 445 (1963).
[36] H. M. Pickett *43rd Symposium on Molecular Spectroscopy*, Ohio State University, Columbus, 1988, paper RD1.
[37] J. T. Hougen and N. Ohashi, J. Mol. Spectrosc. **109**, 134 (1985).
[38] A. S. Pine and B. J. Howard, J. Chem. Phys. **84**, 590 (1986).
[39] N. Moazzen-Ahmadi, A. R. W. McKellar and J. W. C. Johns, Chem. Phys. Lett. (submitted).

Downloaded 08 Mar 2006 to 131.215.225.174. Redistribution subject to AIP license or copyright, see http://jcp.aip.org/jcp/copyright.jsp